11-2019

A Parametric Study for In-Pile Use of the Thermal Conductivity Needle Probe Using a Transient, Multilayered Analytical Model

Courtney Hollar
University of Idaho

Austin Fleming
Idaho National Laboratory

Kurt Davis
Idaho National Laboratory

Ralph Budwig
University of Idaho

Colby Jensen
Idaho National Laboratory

See next page for additional authors

Publication Information

Hollar, Courtney; Fleming, Austin; Davis, Kurt; Budwig, Ralph; Jensen, Colby; and Estrada, David. (2019). "A Parametric Study for In-Pile Use of the Thermal Conductivity Needle Probe Using a Transient, Multilayered Analytical Model". *International Journal of Thermal Sciences, 145*, 106028-1 - 106028-10. https://doi.org/10.1016/j.ijthermalsci.2019.106028

International Journal of Thermal Sciences 145 (2019) 106028

Contents lists available at ScienceDirect

International Journal of Thermal Sciences

journal homepage: www.elsevier.com/locate/ijts

A parametric study for in-pile use of the thermal conductivity needle probe using a transient, multilayered analytical model

Courtney Hollar[a,**], Austin Fleming[b], Kurt Davis[b], Ralph Budwig[a], Colby Jensen[b,***], David Estrada[a,c,*]

[a] Department of Mechanical Engineering, University of Idaho, Boise, ID 83702, United States
[b] Idaho National Laboratory, Idaho Falls, ID 83415, United States
[c] Center for Advanced Energy Studies and Micron School of Materials Science, Boise State University, Boise, ID 83725, United States

ARTICLE INFO

Keywords:
Thermal conductivity
Transient line source method
Uranium dioxide
In-pile instrumentation

ABSTRACT

By utilizing an in-pile measurement, thermal conductivity can be determined under prototypic conditions over a range of burnup. In this work we develop a multilayer quadrupoles analytical model to describe the transient thermal interactions between a line heat source (i.e. needle probe) and cylindrical nuclear fuel geometry for in-pile thermal conductivity measurements. A finite element analysis of the detailed needle probe geometry was compared to results from the analytical model to verify the assumptions made in the analytical model. Experimentally, the needle probe was used to measure the thermal properties of polytetrafluoroethylene (PTFE) and stainless steel 304 with three different diameters (10 mm, 20 mm, and 30 mm). The analytical model was compared to the experimental measurements, which showed good agreement within an average standard error of 0.501 K. Rather than be restricted to the linear region of the temperature v. log(time) slope, the analytical model can use the entire experimental curve to determine the thermal conductivity of the samples. Using the analytical model, a parameter and sensitivity study was conducted to explore the viability of accurately measuring the sample thermal conductivity under various measurement conditions. In addition, three different parameters were studied for optimization: various UO_2 diameters, various probe diameters, and thermal contact resistance. The validated model and results provide the foundation to elucidate a better understanding of in-pile thermal conductivity measurements and informs future needle probe designs to measure samples with diameters as low as 10 mm.

1. Introduction

Knowledge of the thermal conductivity of nuclear fuels can be used to increase the understanding of fuel behavior, support simulation design codes, and to develop advanced fuels. During irradiation, nuclear fuels experience a change in physical structure and chemical composition. Current thermal conductivity measurement approaches for irradiated fuels rely on post irradiation examination (PIE), which can be challenging and is believed to not be fully representative of the state of the fuel while under irradiation in a reactor.

Most PIE methods use the laser-flash technique to determine the thermal conductivity [1–4]. In addition, some studies measure the thermal conductivity using laser-flash at elevated temperatures. However, this approach does not account for a high radiation environment. The Halden Boiling Water Reactor has performed in-pile thermal conductivity measurements by measuring the centerline temperature [5]. Several required assumptions to extract thermal conductivity are not always satisfied including uniform fuel composition, uniform fuel density, minimal thermal contact resistance effects, and uniform heat generation within the fuel rod. For high burnup scenarios, detailed knowledge of fuel properties is difficult to know in many cases. Therefore, in many cases it is impossible to determine if these assumptions are met, and if they are not, estimate a corresponding uncertainty value. In addition, well-known heat flux and thermal hydraulic conditions are required.

The transient line source method is an alternative approach to measuring the thermal conductivity of solids, which has previously been adapted for in-pile applications [6,7]. The detailed technique of

* Corresponding author. Department of Mechanical Engineering, University of Idaho, Boise, ID 83702, United States.
** Corresponding author.
*** Corresponding author.
E-mail addresses: courtneyhollar@boisestate.edu (C. Hollar), colby.jensen@inl.gov (C. Jensen), daveestrada@boisestate.edu (D. Estrada).

https://doi.org/10.1016/j.ijthermalsci.2019.106028
Received 7 March 2019; Received in revised form 8 July 2019; Accepted 16 July 2019

the transient line source is well documented in literature and standards [8]. However, there are also challenges associated with this method. In the standard technique, the sample is assumed to be semi-infinite. Yet, prototypic light water fuels consisting of uranium dioxide (UO_2), have a diameter of approximately 10 mm. In addition, the standard technique assumes that thermal contact resistance is negligible and that the probe is infinitely thin.

Based on the transient line source method, the Idaho National Laboratory (INL) has developed an in-pile transient needle probe which can produce a temperature gradient while measuring the centerline temperature. The needle probe, based on the transient line source method, is a commonly used technique for thermal conductivity measurements. The needle probe developed by Idaho National Laboratory was adapted for high temperature operation, allowing it to be used in nuclear fuels.

This paper establishes a transient, multilayer analytical model that accurately represents the heat transfer between the needle probe, sample, and surrounding environment. This analytical model is compared to a detailed finite element model to demonstrate that the simplified geometry is representative of the needle probe. In addition, experimental results for a variety of sample materials are compared to the analytical model, all within good agreement. Using the analytical model, a sensitivity study is conducted in order to determine the influence of each parameter during the thermal conductivity measurement using the needle probe. From here, recommendations are made in order to optimize the needle probe for measurement of prototypic light water fuels.

2. Theory

The transient needle probe consists of a heater and a thermocouple. The distance between the heater and thermocouple are typically 0.17 mm. Fig. 1 shows the cross-section view of the needle probe. The probe utilizes a line heat source that is embedded into the sample in order to determine the thermal conductivity. When the sample is at thermal equilibrium, a step-function in power is supplied to the heater and the thermocouple records the sample's temperature response. The temperature response of the sample is dependent on the thermal properties and geometry. As a result, the thermal conductivity can be calculated from the temperature rise within the sample. This transient measurement method traditionally utilizes the linear region of the temperature versus the natural logarithm of time in order to determine the thermal conductivity. The linear region corresponds to a time scale

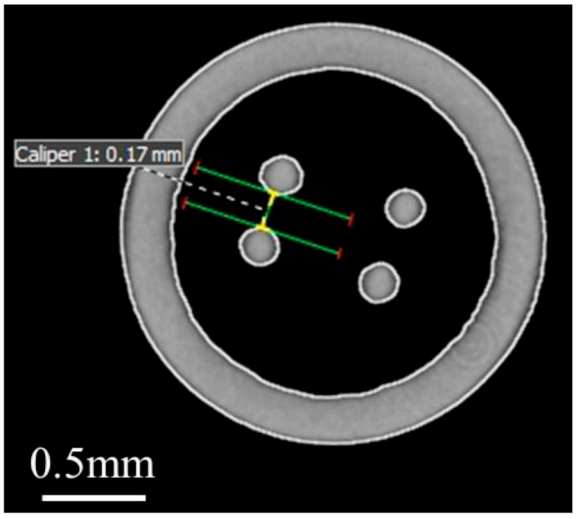

Fig. 1. X-Ray Micro-CT cross-section of the needle probe showing insulation, sheath, thermocouple wires, and heater wires.

in which the sample appears to be semi-infinite, thereby eliminating the dependence on sample geometry.

The needle probe method uses the theory of an infinite line heat source that is embedded in a semi-infinite solid. As a result, the thermal response is detected by a thermocouple that is located a finite distance from the heater. In this case, INL developed a probe that houses both the heater and thermocouple within one probe. The thermal conductivity is then derived using the equation according to the ASTM needle probe testing standard [9]:

$$k = \frac{Q_0}{4\pi LS}, \tag{1}$$

where k, Q_o, L, and S are the thermal conductivity, power dissipated by the heater, heater length, and slope of the linear portion of the transient response, respectively. The slope of the linear region of the temperature versus the natural logarithm of time is defined as:

$$S = \frac{\partial T}{\partial \ln(t)}, \tag{2}$$

where T and t are the temperature and time, respectively.

In addition, use of the needle probe method requires an understanding of the probe and sample's Fourier number. The Fourier number is defined as:

$$Fo = \frac{\alpha t}{R^2} \tag{3}$$

where α, t, and R is the thermal diffusivity, time, and characteristic length, respectively.

The probe's Fourier number was calculated based on the probe's effective thermal diffusivity, the time at which the temperature v. time curves enter the 5% linear region, and the outer radius of the probe. Based upon these calculations, the probe's Fourier number must be greater than 330 in order to allow for enough time for the heat to move out of the probe.

Furthermore, the sample's Fourier number was calculated based on the sample's thermal diffusivity, the time at which the temperature v. time curves left the 5% linear region, and the outer radius of the sample. The Fourier number of various samples including PTFE and UO_2 validates that the Fourier number is independent of individual material properties. As a result, the sample's Fourier number needs to be smaller than 0.2 in order to prevent the heat from reaching the outer surface.

This needle probe method uses the assumption of a semi-infinite sample; however nuclear fuel samples of interest are about 10 mm in diameter. Therefore, it is necessary to select a very specific time interval in order to ensure an accurate thermal conductivity measurement. A model is needed that will facilitate understanding of the impact of a finite specimen boundary condition as well as the effects of a potentially significant thermal contact resistance between the probe and sample.

3. Literature review

A literature review was performed to determine if a 1-D radial, transient analytical model has already been developed for this scenario. One publication used the Jaeger theory to develop an analytical model, however differences between experimental data and the analytical model were observed before 500 s [10]. It was then discovered that ground heat exchangers used in the geoscience field applied closely to this problem. Ground heat exchangers are cylindrical pipes that dissipate excess heat into the soil. This is analogous to the needle probe. In addition, the soil is essentially the nuclear sample while the backfill is the thermal grease. Since ground heat exchangers are designed to be used for several decades, the shortest time responses were modelled for a few days or minutes [11–13]. Alternative models focused on understanding the 2-D heat flow as a result of a U-shaped ground heat

exchanger [14] while others had interest in only determining the temperature distribution within the ground heat exchanger or within the backfill [15–17]. Several publications have acknowledged the difficulty of solving this problem as a result of the transient state and complex boundary conditions. Therefore, they turned to finite difference and numerical solutions [11,13,18].

One publication, written by Gu [19], developed a dimensionless solution for a constant cylindrical heat source for a medium composed of backfill and soil. The basic heat conduction equation was put into non-dimensional form while the orthogonal expansion technique consisting of eigenvalues and eigenfunctions was used to solve for the temperature distribution. Bandyopadhyay et al. stated that Gu's approach has experienced disagreement in the community of heat conduction researchers [20–22]. In this paper, the method of thermal quadrupoles was used to derive a flexible model of the needle probe and sample system.

4. Quadrupoles method

The theoretical model derived here is based on a two layer system, though adding additional layers is quite simple. The first layer represents probe properties and the second represents the sample with a contact resistance between the layers and convection occurring on the outer surface of the sample. Fig. 2a shows a schematic cross-section of the needle probe inserted into the centerline of a sample. Various parts of the needle probe are included such as the outer sheath, insulation, thermocouple wires, and the heater wires. This analytical model serves as a tool to understand each parameter and its influence on the thermal conductivity accuracy. The analytical model assumes that the probe is one layer, as a result, this requires the use of an effective thermal diffusivity and thermal conductivity of the probe rather than developing a detailed probe that includes the individual components outer sheath, insulation, thermocouple wires, and heater wires. Fig. 2b shows the equivalent geometry chosen to represent the needle probe geometry, which is embedded into the centerline of the sample, used in the analytical model.

To account for the influence of the sheath, insulation, thermocouple wires, and heater wires, the effective thermal capacity and thermal conductivity of the probe are accounted for using equations (4) and (5)

$$(\rho c_p)_{eff} = \frac{A_{wires}(\rho c_p)_{wires} + A_{ins}(\rho c_p)_{ins} + A_{sheath}(\rho c_p)_{sheath}}{A_{probe}} \tag{4}$$

$$k_{eff} = \frac{\ln\left(\frac{r_{sheath}}{r_{wires}}\right)}{\frac{\ln\left(\frac{r_{ins}}{r_{wires}}\right)}{(k_{ins})} + \frac{\ln\left(\frac{r_{sheath}}{r_{ins}}\right)}{(k_{sheath})}} \tag{5}$$

where ρ, c_p, A, k, r_{wires}, r_{ins}, and r_{sheath} are the density, specific heat, cross-sectional area, thermal conductivity, outer radius of wires, outer radius of insulation, and outer radius of sheath, respectively. The assumption for using the resistor analogy in order to determine the effective thermal conductivity is that there is no heat generation and the heat flow is one-dimensional.

Using these effective thermal properties, an analytical solution can be developed to model the needle probe when inserted into the centerline of a cylindrical nuclear fuel pellet. The quadrupoles method is an exact explicit method that represents a linear system [23]. This method can be used to determine the temperature field in multilayered materials using direct solutions to the heat diffusion equation. In order to use the quadrupoles method, the temperature and heat flux must be transformed into the Laplace temperature (θ) and Laplace heat flux (φ). A matrix is developed for the probe, thermal contact resistance, sample, and convection. Using matrix multiplication, a solution can be easily constructed for the multilayered system. Equations (6) and (7) were used to develop the matrix system of the probe and sample in cylindrical coordinates [23].

$$q_{1,i} = r_i\sqrt{p/\alpha_i} \quad q_{2,i+1} = r_{i+1}\sqrt{p/\alpha_i} \tag{6}$$

$$A_i = q_{2,i}[I_0(q_{1,i})K_1(q_{2,i}) + I_1(q_{2,i})K_0(q_{1,i})] \tag{7a}$$

$$B_i = \frac{1}{2\pi kL}[I_0(q_{2,i})K_0(q_{1,i}) - I_0(q_{1,i})K_0(q_{2,i})] \tag{7b}$$

$$C_i = 2\pi kLq_{1,i}q_{2,i}[I_1(q_{2,1})K_1(q_{1,i}) - I_1(q_{1,i})K_1(q_{2,i})] \tag{7c}$$

$$D_i = q_{1,i}[I_0(q_{2,i})K_1(q_{1,i}) + I_1(q_{1,i})K_0(q_{2,i})] \tag{7d}$$

where r is the radius of each layer, p is the Laplace parameter, α is thermal diffusivity, k is thermal conductivity, L is the length of the cylinder, I_0 is a modified Bessel function of the first kind of order 0, I_1 is a modified Bessel function of the first kind of order 1, K_0 is a modified Bessel function of the second kind of order 0, and K_1 is a modified Bessel function of the second kind of order 1. The subscript i corresponds to the layer in the model (1 being the probe, 2 being the sample).

Equation (8) shows the matrix representation of a one-layered cylindrical material

$$\begin{bmatrix}\theta_1\\ \varphi_1\end{bmatrix} = \begin{bmatrix}A_1 & B_1\\ C_1 & D_1\end{bmatrix}\begin{bmatrix}\theta_2\\ \varphi_2\end{bmatrix} \tag{8}$$

where θ and φ are the Laplace temperature and Laplace heat flux, respectively. This matrix can be used to represent the probe layer and the sample layer.

Equation (9) shows the matrix representation of a thermal contact interface

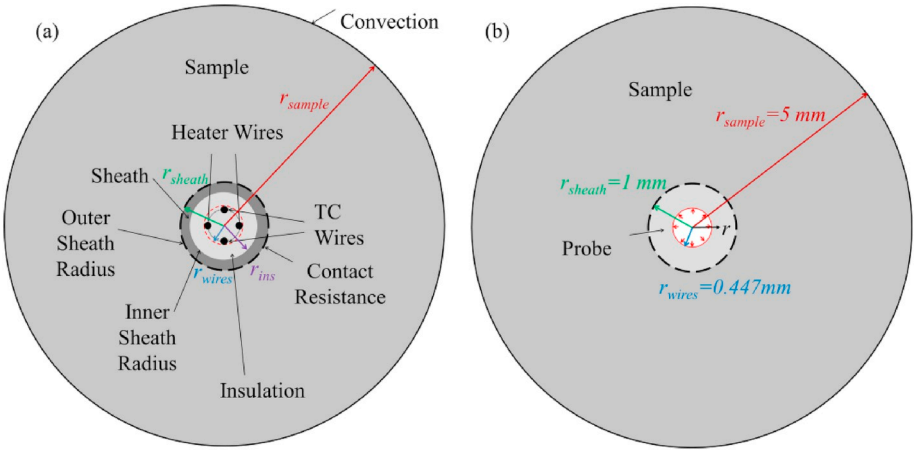

Fig. 2. (a) Diagram of the needle probe geometry inserted into a cylindrical sample. (b) diagram of the equivalent heat transfer geometry.

$$\begin{bmatrix}\theta_1\\ \varphi_1\end{bmatrix} = \begin{bmatrix}1 & R_{th}\\ 0 & 1\end{bmatrix}\begin{bmatrix}\theta_2\\ \varphi_2\end{bmatrix} \quad (9)$$

where R_{th} is the thermal contact resistance. This matrix can be used to represent the thermal contact resistance layer. The thermal contact resistance takes into account the influence of small air gaps that are associated with the machining tolerances and the imperfect contact due to the surface roughness. This contact resistance is independent of thermal conductivity since it is accounting for the complex heat transfer between the conduction layers.

Equation (10) represents the entire needle probe-thermal contact resistance-nuclear fuel-convection multilayered system.

$$\begin{bmatrix}\theta_1\\ \varphi_1\end{bmatrix} = \begin{bmatrix}A_1 & B_1\\ C_1 & D_1\end{bmatrix}\begin{bmatrix}1 & R_{th}\\ 0 & 1\end{bmatrix}\begin{bmatrix}A_2 & B_2\\ C_2 & D_2\end{bmatrix}\begin{bmatrix}1 & 0\\ h & 1\end{bmatrix}\begin{bmatrix}\theta_3\\ \varphi_3\end{bmatrix} \quad (10)$$

where h is the convection coefficient associated with the boundary condition of convection at the outer surface of the sample. The temperature response of the probe, θ_1, can then be calculated by expanding the matrix into equation form since there are two unknowns and two equations. A Laplace inversion is then performed to transform the temperature response of the probe θ_1 into T_1.

The quadrupoles analytical solution model, hereafter called the analytical model, was compared to a finite element software model. A finite element model was created using the detailed geometry and thermal properties of the probe while another finite element model used the equivalent heat transfer geometry and thermal properties for comparison. All models use the thermal properties and geometry of a 10 mm diameter UO_2 sample, with the boundary conditions of a constant heat flux at the centerline and convection at the outer surface of the sample. The finite element models were conducted using COMSOL Multiphysics. The mesh was created by COMSOL using the extra fine setting to adequately resolve the features internal to the probe. As can be seen in Fig. 3a and b, good agreement, with a standard error of 0.0039 K, was achieved which provides verification of the solution and validates use of the lumped thermal properties of the probe.

5. Results and discussion

5.1. Methods

Experimental validation of the analytical model was performed using a custom-built needle probe. The effective thermal diffusivity and thermal conductivity of the probe were calculated to be 1.37e-5 m^2/s and 42 W/m K, respectively. The thermal diffusivity and thermal conductivity literature values of the thermocouple wires, heater wires, insulation, and sheath were used to calculate the effective properties based on the appropriate temperature. Varying temperature ranges will affect the effective thermal diffusivity and thermal conductivity values. The individual thermal diffusivity of the thermocouple wires, heater wires, insulation, and sheath were weighted based on volume and then summed together to result in the effective thermal diffusivity of the probe. Furthermore, the effective thermal conductivity of the probe was calculated using the thermal resistor analogy, as defined in equations (4) and (5). Cylindrical polytetrafluoroethylene (PTFE) and stainless steel 304 were selected as the test materials to provide a broad thermal conductivity range of 0.25 W/m K to 14.8 W/m K. Furthermore, various outer diameters of 10 mm, 20 mm, and 30 mm were selected to determine the influence of the samples' outer boundaries.

All testing of samples were performed in an ambient room temperature environment of 20 °C. The power supplied to the needle probe ranged from 1 to 10 W. The temperature history was collected using a custom LabView program. Experiments were performed for approximately 1000 s in order to demonstrate the analytical models to predict all stages of the temperature v. log(time) curve. Consecutive measurements were performed once the samples reached room temperature.

The heating of the needle probe causes a small temperature rise on the outer surface of the sample, which drives some natural convection in addition to conduction to the surrounding air. In the analytical model this boundary is treated as convection to the ambient temperature.

A hole of 2.06 mm was pre-drilled into the centerline of the calibration materials in order for a 2.01 mm diameter needle probe to be easily inserted. Since the probe and sample were not pressure fit, the thermal contact resistance between the probe and medium were relatively large (i.e. 0.6 K m^2/W to 2 K m^2/W).

The thermal contact resistance, thermal conductivity, and thermal diffusivity values for each sample was determined by adjusting the temperature v. time curve of the analytical model until it matched the entire experimental temperature v. time curve. These thermal properties were determined independently for each sample and experiment.

5.2. PTFE

Fig. 4a shows that all three PTFE samples exhibited the same trend for the first 20 s. Afterwards, the boundary conditions begin to affect the 10 mm diameter sample. At approximately 200 s, the heat has

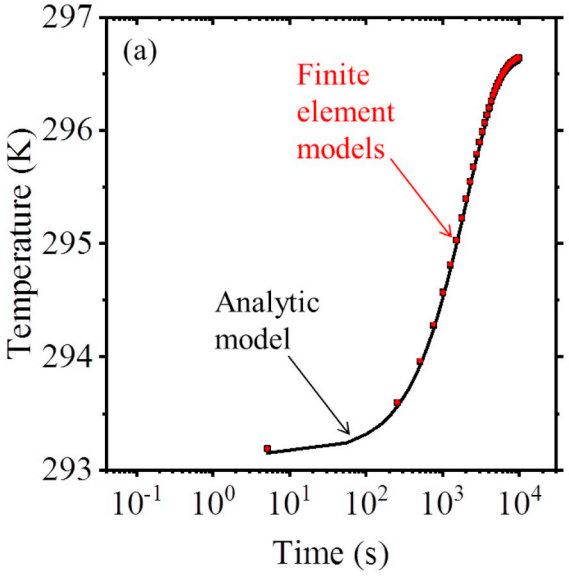

(b)

r_{wires} (mm)	0.447
r_{sheath} (mm)	1
r_{sample} (mm)	5
α_{probe} (m^2/s)	1.37e-5
k_{probe} (W/m·K)	42
α_{UO2} (m^2/s)	6.2e-7
k_{UO2} (W/m·K)	2.5
Length (m)	0.2
Contact resistance (K·m^2/W)	1
h (W/m^2·K)	10
Q (W)	10

Fig. 3. (a) Temperature v. time plot for the analytical solution based on the equivalent heat transfer geometry and finite element model using both the detailed geometry and thermal properties and the equivalent heat transfer geometry and thermal properties. The finite element models are dotted while the analytical model is the solid black line. (b) Table of thermal properties and geometry of probe inserted into the centerline of a UO_2 sample.

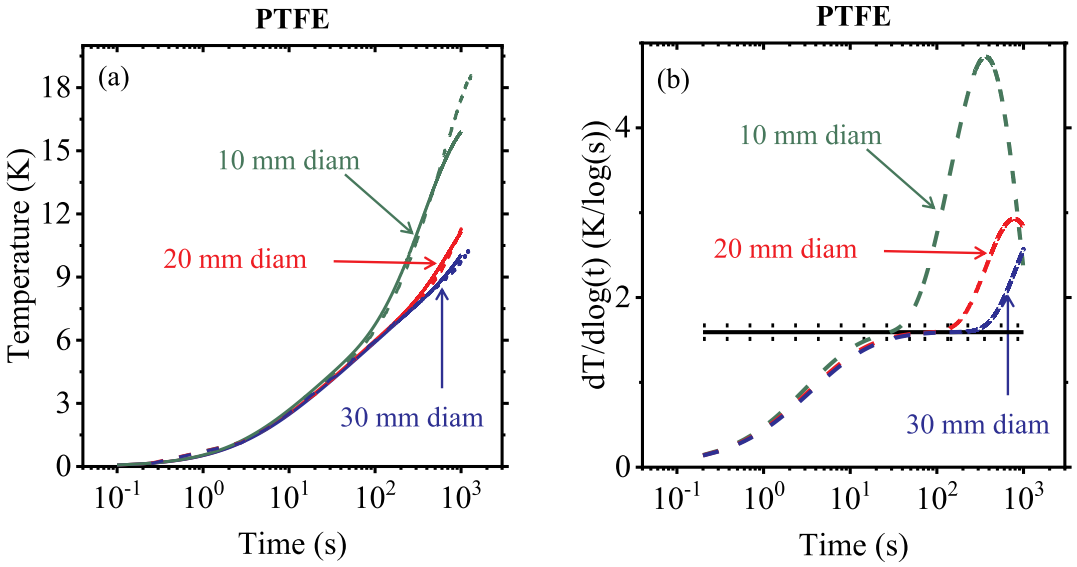

Fig. 4. (a) Temperature v. time plot of PTFE samples with various diameters of 10 mm, 20 mm, and 30 mm. Dashed lines indicate analytical model and solid lines indicate experimental data. (b) derivative of the temperature v. log(t) plot versus time. The ±5% of the known thermal conductivity value are the two black dashed lines while the known thermal conductivity value according to literature is the solid black line.

travelled through the entire 20 mm diameter sample. The analytical model and experimental results show good agreement while the heat is travelling through the sample. Once the heat meets the outer boundary, convection begins to dominate the temperature change. Using the model to match the entire experimental data curve, the thermal diffusivity and thermal conductivity of PTFE used in Fig. 4a, were determined to be 1.24e-7 m^2/s and 0.25 W/m K, respectively, for measurements performed at 293 K. This demonstrates good agreement with the literature values for PTFE, where thermal conductivity is 0.25 W/m K at 296 K [24] and thermal diffusivity is 1.24e-7 m^2/s at 293 K [25]. If the thermal conductivity were to be calculated using the slope of the linear region of the temperature versus the natural logarithm of time the 10 mm, 20 mm, and 30 mm diameter samples would exhibit linearity from 16 s to 38 s, 26 s to161s, and 29 s to354 s, respectively. This was determined by graphing the derivative of the temperature v. log (time) plot versus time (Fig. 4b). The known thermal conductivity of PTFE was then graphed which included a 5% thermal conductivity range. The 5% thermal conductivity range are the two black dashed lines within the plot that indicate ±5% of the known thermal conductivity value while the solid black line is the known thermal conductivity value. The linear region of the temperature versus the natural logarithm of time was then found to be when the curve was within the 5% thermal conductivity range. This indicates that samples with a smaller diameter have a smaller linear region due to the heat quickly travelling to the outer surface resulting in boundary effects.

The thermal contact resistance range for the PTFE samples was 0.6 K m^2/W to 1 K m^2/W. This range in thermal contact resistances for the same material can be attributed to the machining tolerance associated with the diameter of the hole.

Overall, using the analytical model demonstrates that the semi-infinite assumption is not required, which allows prototypic samples to be measured. This is due to the good agreement achieved for the entire time range between the experimental and analytical model curves. Since the analytical model takes into account the initial time when the heater is turned on until convection begins to dominate, this approach is no longer restricted to using only the linear region of the temperature v. log(time) slope.

5.3. Stainless steel 304

Similar experiments were also performed on stainless steel 304 samples, as shown in Fig. 5. As a result of the higher thermal conductivity as compared to the PTFE, the heat travelled faster to the outer surface. Furthermore, the thermal contact resistance for the stainless steel 304 samples ranged between 1.35 K m^2/W to 2 K m^2/W. As a result of the relatively large thermal contact resistance, it can be seen that from 3 s to 10 s there is an additional curve which does not occur in the PTFE measurements. In comparison to the thermal contact resistance for the PTFE samples, stainless steel 304 samples exhibit a higher thermal contact resistance. This can be attributed to the machining tolerances associated with the diameter of the hole. Furthermore, there is variation in the surface roughness of the different materials and PTFE is more compliant. Therefore, there is a difference in contact with the probe for same diameter samples. Regardless, the analytical model curve is able to exhibit good agreement with the entire experimental curve for each sample. The thermal diffusivity and thermal conductivity used in Fig. 5a, as determined using the analytical model, was 3.8e-6 m^2/s and 14.8 W/m K, respectively, for measurements performed at 293 K. This shows good agreement with stainless steel 304 literature values for a thermal conductivity of 14.34 W/m K at 304 K [26] and a thermal diffusivity of 3.75e-6 m^2/s at 297 K [27]. In this case, we were able to determine the thermal properties by matching the entire curve of the analytical model to the experimental curve. However, trying to determine the thermal conductivity using the slope of the linear region of the temperature versus the natural logarithm of time would not be possible as none of these curves enter the 5% thermal conductivity region (Fig. 5b). Therefore, this demonstrates the quadrupoles model can be used to determine the thermal conductivity of samples that would not typically be accurately measured using the traditional transient line source method. In addition to accurately extracting the correct thermal properties for the sample, the model accurately predicts the temperature response in the time scales in which the sample is not semi-infinite. Specifically, in the short time scales, which is dominated by the probe properties, and the long time scales which is influenced by the boundary conditions and sample radius.

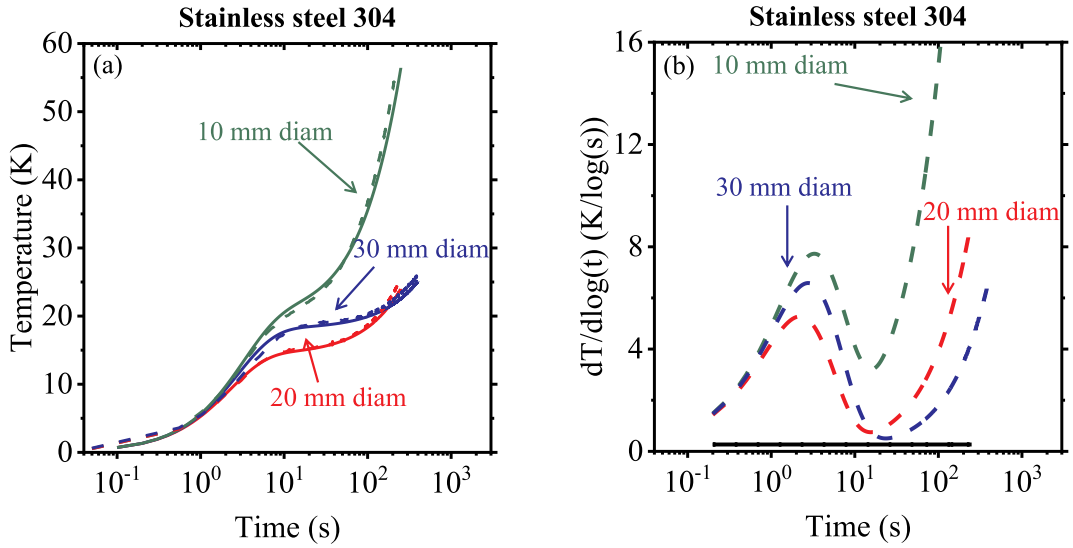

Fig. 5. Temperature v. time plot of stainless steel 304 samples with various diameters of 10 mm, 20 mm, and 30 mm. Dashed lines indicate analytical model and solid lines indicate experimental data. (b) derivative of the temperature v. log(t) plot versus time.

Table 1
Thermal conductivity and thermal diffusivity of PTFE and stainless steel 304 samples.

Material	Thermal conductivity (W/m K)	Thermal diffusivity (m^2/s)
PTFE	0.25 at 293 K	1.24e-7 at 293 K
PTFE	0.25 at 296 K [23]	1.24e-7 at 293 K [24]
SS304	14.8 at 293 K	3.8e-6 at 293 K
SS304	14.34 at 304 K [25]	3.75e-6 at 297 K [26]

A summary of the thermal conductivity and thermal diffusivity for both the PTFE and stainless steel 304 samples are shown in Table 1. All sample diameters for each material exhibited the same thermal conductivity and thermal diffusivity, regardless of size.

5.4. Thermal contact resistance

In order to further understand the influence of the thermal contact resistance, experiments were performed on the stainless steel 304 samples with thermal grease. Fig. 6 shows the influence of the thermal contact resistance on 10 mm, 20 mm, and 30 mm diameter stainless steel 304 samples. The use of thermal grease significantly reduced the thermal contact resistance from an average of 1.68 K m^2/W to 0.53 K m^2/W. Good agreement was obtained across various sized samples utilizing thermal grease, highlighting the impact the air gap can have on the variability of the thermal contact resistance which we associate with machining tolerances.

For this range of thermal contact resistances, the thermal properties of the samples can be accurately determined. Furthermore, this demonstrates that the quadrupoles model shows good agreement with an average standard error of 0.501 K for all PTFE and stainless steel 304 experiments. This indicates that this approach can be used for a range of thermal conductivity values and thermal contact resistances. Moreover, multiple experiments were performed for both the PTFE and stainless steel 304 samples. These replicate temperature v. log(time) curves showed no visible differences.

5.5. Convection

The convection coefficient used in the model was experimentally determined for the stainless steel 304 samples and calculated using the experimental temperature v. time data and the lumped capacitance equation:

$$h = -\frac{\rho V c t}{A_s} ln\left(\frac{T - T_\infty}{T_i - T_\infty}\right) \quad (11)$$

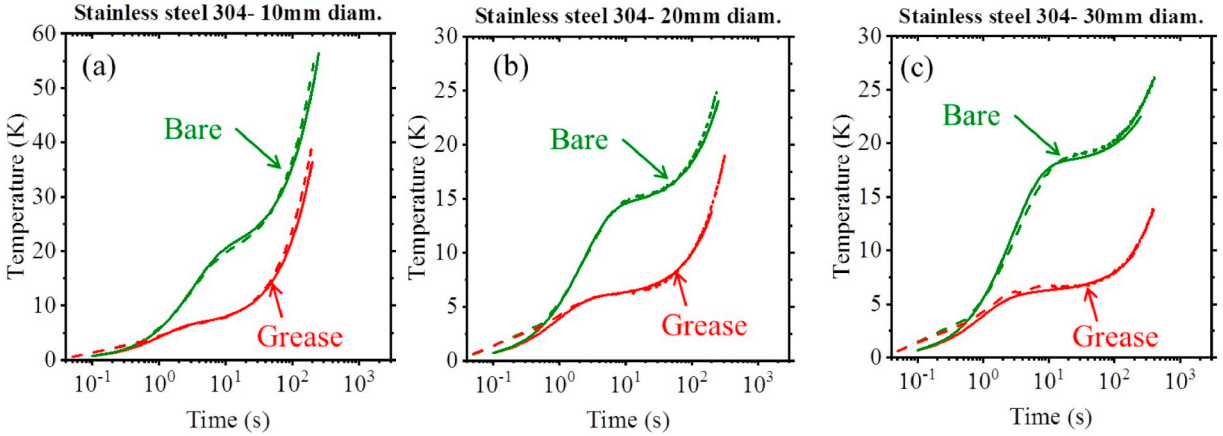

Fig. 6. Temperature v. time plot comparing bare needle probe and thermal greased needle probe for stainless steel 304 samples with a diameter of (a) 10 mm, (b) 20 mm, and (c) 30 mm. Dashed lines indicate analytical model and solid lines indicate experimental data.

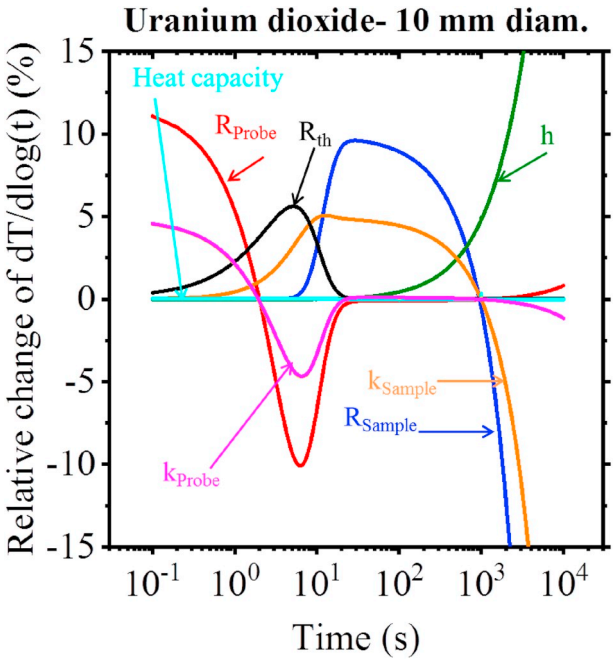

Fig. 7. Relative change v. time plot for 10 mm diameter UO_2 sample comparing probe radius (R_{probe}), thermal conductivity of probe (k_{probe}), thermal contact resistance (R_{th}), sample radius (R_{sample}), thermal conductivity of sample (k_{sample}), convection (h), and various probe thermal properties.

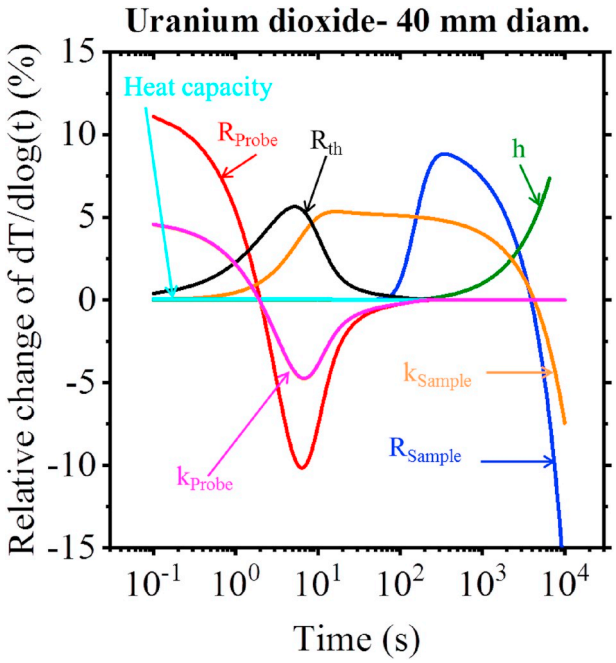

Fig. 8. Relative change v. time plot for 40 mm diameter UO_2 sample comparing probe radius (R_{probe}), thermal conductivity of probe (k_{probe}), thermal contact resistance (R_{th}), sample radius (R_{sample}), thermal conductivity of sample (k_{sample}), convection (h), and various probe thermal properties.

Where h, ρ, V, c, t, A_s, T, T_∞, and T_i are the convection coefficient, density, volume, specific heat, time, surface area, temperature, ambient temperature, and initial temperature. A lumped capacitance model was used while the sample cooled down in order to provide an estimation of the convection coefficient. The Biot number calculated for stainless steel was 0.0017 while the Biot number for PTFE was 0.1.

5.6. Sensitivity parameter study

Based on the verification and validation, a sensitivity parameter study using the analytical model was then performed in order to determine how each parameter influenced the thermal conductivity measurement using the needle probe. As a baseline condition, sample properties for UO_2 were used. The parameters that were varied in this study include thermal contact resistance, probe radius, sample radius, probe thermal conductivity, sample thermal conductivity, convection, and various combinations of the probe's thermal properties. The data reduction technique to determine the thermal conductivity using the needle probe relies on the slope of the T v. log(t) plot, therefore the sensitivity of this slope is of more interest rather than the sensitivity of the temperature. Each parameter was adjusted by 5% of its original value and the percentage of relative change of dT/dlog(t) was used to determine the sensitivity.

Fig. 7 shows for the measurement of a UO_2 sample with a 10 mm diameter, the probe thermal conductivity and probe radius are initially the most sensitive. For example, at 0.3 s, there is a relative slope change of 9.7% and 4.0% for the probe radius and probe thermal conductivity, respectively. This can be attributed to the thermal response of the probe. However, change in the heat capacity results in a negligible relative slope change. Shortly after the heat begins to travel from the probe to the sample, the thermal contact resistance becomes more sensitive. From there, the sample's radius and thermal conductivity dominate after 10 s until the convective losses influence the result.

The UO_2 diameter was then increased to 40 mm to see if the sample's thermal conductivity could be isolated to enhance sensitivity during measurements. Fig. 8 shows the probe's thermal response is still the most sensitive initially. As the heat begins to move outward from the probe to the sample the thermal contact resistance increases in sensitivity. The heat continues to travel through the sample and the sample's radius and thermal conductivity become more sensitive between 10 s and 2000 s. This becomes the ideal measurement region because the response of the sample's thermal conductivity and radius are more sensitive compared to other parameters. Furthermore, the sample's radius can be accurately determined, which allows for calculation of the sample's thermal conductivity. Therefore, a sample with a diameter greater than 40 mm is sufficient in order to optimize the measurement region by isolating the sample's thermal conductivity sensitivity while other parameters exhibit a low sensitivity.

5.7. Uranium dioxide

Using the thermal contact resistance and convection coefficients determined experimentally, the analytical model will be used to simulate experiments on UO_2 samples of various diameters. These results will inform the expected quality of experimental results that can be obtained from UO_2 samples. Additionally, these results can be used to aid in the design of an experiment to ensure good thermal conductivity measurements. Fig. 9a shows the simulated temperature v. time plot for a varying diameter of 20 mm, 40 mm, and 60 mm. Fig. 9b shows the dT/dlog(t) v. time graph, where the solid black line is the slope that corresponds to the thermal conductivity of UO_2 and the two dashed black lines are the slopes that correspond to ±5% of the UO_2 thermal conductivity. For a 20 mm diameter, the dT/dlog(t) curve never enters the 5% thermal conductivity range. If the standard data reduction technique of fitting the linear region for the slope was used for this data, it would not have obtained an accurate measurement because the semi-infinite assumption was not satisfied. However, a 40 mm diameter remains within the 5% thermal conductivity range from 37 s to 124 s. This indicates that UO_2 can have a minimum diameter of 40 mm while still remaining within the 5% thermal conductivity range for a sufficient amount of time. This further confirms the previous sensitivity parameter plots that a 40 mm diameter of UO_2 is the sufficient sample size for the current needle probe being used, if the standard data reduction procedure is used. The derived analytical model could be used to fit the

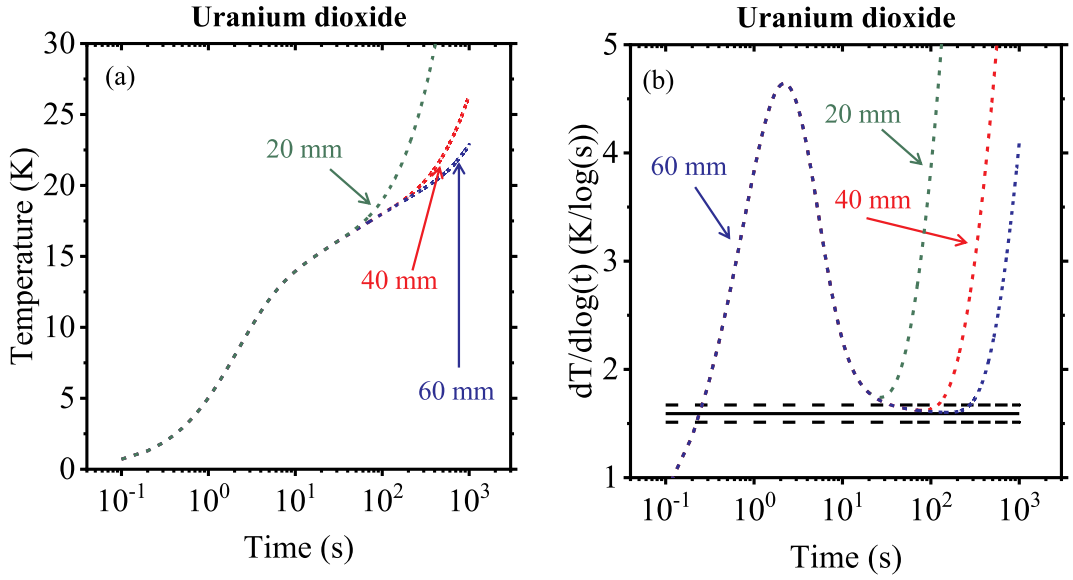

Fig. 9. (a) Temperature v. time plot and (b) dT/dlog(t) plot comparing the minimum diameter of UO_2 samples.

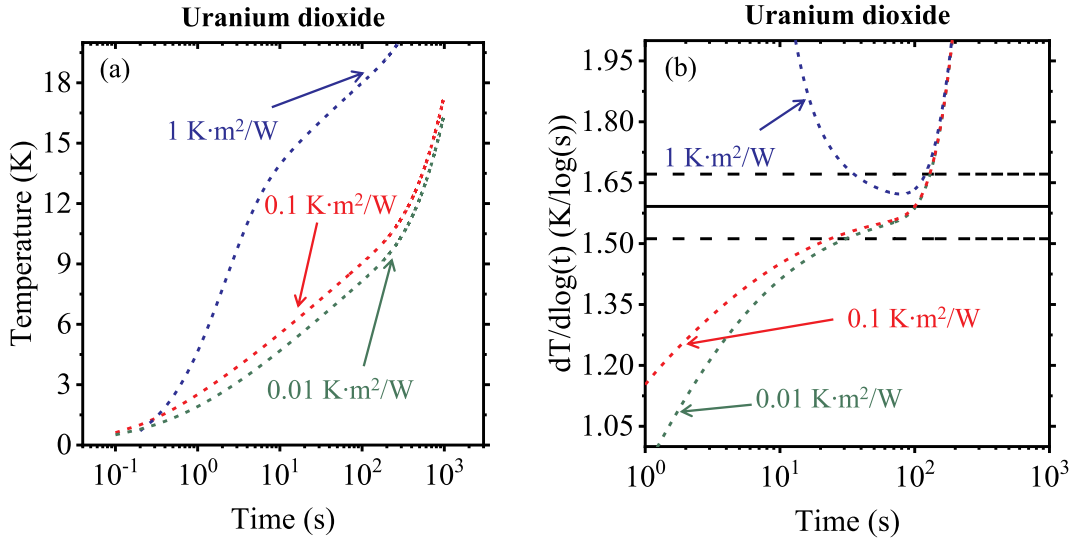

Fig. 10. (a) Temperature v. time plot and (b) dT/dlog(t) plot comparing the smallest thermal contact resistance for a 40 mm diameter UO_2 sample.

thermal properties of the sample to the experimental data without using the standard data reduction technique. This technique is a standard method to determine properties through the inverse problem, and is routinely performed with thermal wave techniques [28,29].

The influence of thermal contact resistance between the needle probe and UO_2 was also investigated using the analytical model. Fig. 10a shows the thermal contact resistances of 0.01 K m^2/W, 0.1 K m^2/W, and 1 K m^2/W. Thermal contact resistance of 0.01 K m^2/W and 0.1 K m^2/W stay within the 5% thermal conductivity range for approximately the same amount of time. Meanwhile 1 K m^2/W does not stay within the 5% thermal conductivity range for a sufficient amount of time (Fig. 10b). Therefore, any contact resistance less than 0.1 K m^2/W can be considered negligible for this set of geometry and material properties.

Another approach to improving the thermal conductivity measurement method is to use a smaller needle probe diameter. Fig. 11a shows that for a 40 mm diameter UO_2 sample, a probe diameter of 0.2 mm allows for the measurement to remain within the 5% thermal conductivity range for the longest time period (Fig. 11b). This indicates that the smaller the probe becomes, it begins to more closely model a true line heat source and will remain within the 5% thermal conductivity range for a longer amount of time. This indicates that, if the needle probe could be miniaturized, it could be used on smaller diameter samples.

6. Conclusions

This study has developed a quadrupoles model that can be used to predict the needle probe measurement process for materials of various thermal conductivities. The model is especially important for applications to multilayered systems with thermal contact resistance and finite size. This analytical model was verified with a finite element software model. Validation was performed using a custom built probe and cylindrical PTFE and stainless steel 304 samples of varying diameters. The analytical model was used to fit the experimental data to determine the thermal conductivity, showing a good agreement with an average standard error of 0.501 K for all PTFE and stainless steel 304 experiments. This demonstrates that the analytical model can be used to

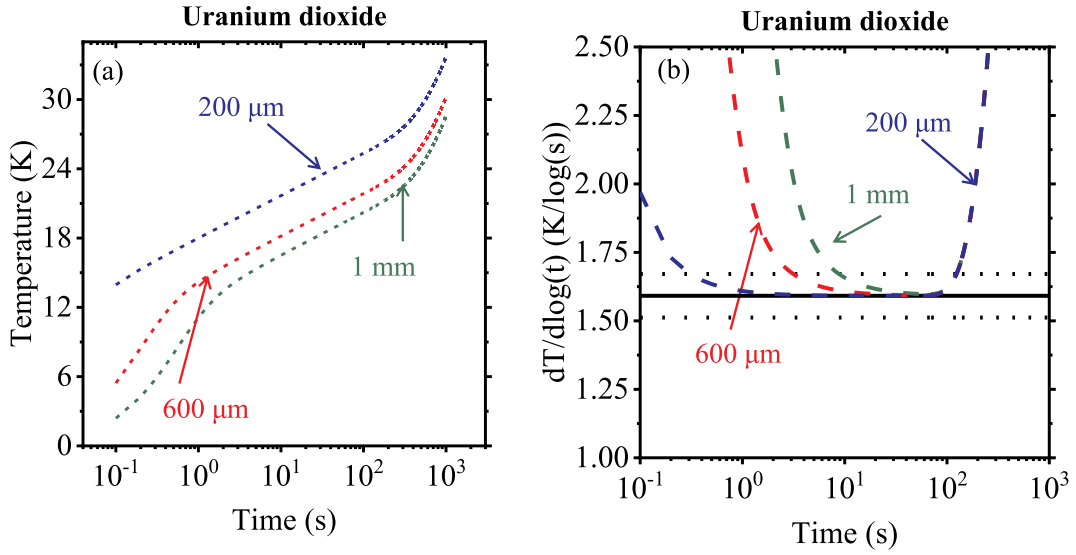

Fig. 11. (a) Temperature v. time plot and (b) dT/dlog(t) plot comparing smaller needle probe diameters for a 40 mm diameter UO_2 sample.

determine the thermal properties of various samples based on matching the entire temperature v. log(time) curve to the experimental results. A sensitivity parameter study was then performed to understand how each parameter influences the thermal conductivity measurement when using the needle probe. It has also shown potential to help optimize the current needle probe thermal conductivity measurement configuration.

For prototypic UO_2 nuclear fuel, the semi-infinite assumption typically required for the standard line source technique is quickly violated during a measurement. However, using a more complex data reduction with the developed analytical model, the thermal conductivity may be determined, though care must be taken to ensure unique fitting solutions for thermal conductivity. The sensitivity studies on various parameters shows a large region of time when the sample's radius and thermal conductivity have a high sensitivity. Therefore, it is possible to determine the thermal conductivity of samples that have a known diameter by fitting the thermal response. The results indicate promise for measuring samples that have a diameter of approximately 10 mm.

Experimental and analytical studies with the current needle probe geometry show that the thermal contact resistance and probe size are the most limiting factors to improving measurements. It has been shown that the thermal contact resistance should be no larger than 0.1 $K\,m^2/W$ to have a negligible influence on the thermal conductivity measurements. In addition, using a smaller probe diameter could increase the amount of time spent within the 5% thermal conductivity range.

Conflicts of interest

The authors have no competing interests to declare.

Declarations of interest

None.

Funding

Courtney Hollar was partially supported by the National Science Foundation Graduate Research Fellowship Program under Grant No. 1545659. This work was supported through the Department of Energy In-Pile Instrumentation program, under DOE Idaho Operations Office Contract DE-AC07-05ID14517.

Appendix A. Supplementary data

Supplementary data to this article can be found online at https://doi.org/10.1016/j.ijthermalsci.2019.106028.

References

[1] C. Ronchi, M. Sheindlin, D. Staicu, M. Kinoshita, Effect of burn-up on the thermal conductivity of uranium dioxide up to 100.000 MWdt−1, J. Nucl. Mater. 327 (1) (2004) 58–76 https://doi.org/10.1016/j.jnucmat.2004.01.018.
[2] S. Ishimoto, M. Hirai, K. Ito, Y. Korei, Effects of soluble fission products on thermal conductivities of nuclear fuel pellets, J. Nucl. Sci. Technol. 31 (8) (1994) 796–802, https://doi.org/10.1080/18811248.1994.9735225.
[3] M. Hirai, Thermal diffusivity of UO2-Gd2O3 pellets, J. Nucl. Mater. 173 (3) (1990) 247–254 https://doi.org/10.1016/0022-3115(90)90392-Z.
[4] M.J. Welland, R. Böhler, L. Vlahovic, K. Boboridis, D. Manara, Co-development of experimental and simulation methods for the laser flash heating and melting technique: the thermoelastic effects of UO2, Int. J. Therm. Sci. 132 (2018) 174–185 https://doi.org/10.1016/j.ijthermalsci.2018.05.035.
[5] W. Wiesenack, T. Tverberg, The OECD Halden reactor project fuels testing programme: methods, selected results and plans, Nucl. Eng. Des. 207 (2) (2001) 189–197 https://doi.org/10.1016/S0029-5493(00)00385-X.
[6] D. Joshua, et al., Hot Wire Needle Probe for In-Pile Thermal Conductivity Detection, United States (2001) [Online]. Available: https://www.osti.gov/servlets/purl/1004270.
[7] J.L. Rempe, et al., Advanced in-pile instrumentation for materials testing reactors, IEEE Trans. Nucl. Sci. 61 (4) (Aug. 2014) 1984–1994, https://doi.org/10.1109/TNS.2014.2335616.
[8] A.E. Wechsler, The probe method for measurement of thermal conductivity, Compendium of Thermophysical Property Measurement Methods, Springer, 1992, pp. 161–185.
[9] Standard Test Method for Determination of Thermal Conductivity of Soil and Soft Rock by Thermal Needle Probe Procedure, ASTM International, 2008 ASTMD Standard 5334-08.
[10] L. Marmoret, H. Humaish, Limit of validity of the log-linear model for determining thermal properties of light insulation materials with cylindrical hot probe, Int. J. Therm. Sci. 117 (2017) 251–259 https://doi.org/10.1016/j.ijthermalsci.2017.04.002.
[11] H. Demir, A. Koyun, G. Temir, Heat transfer of horizontal parallel pipe ground heat exchanger and experimental verification, Appl. Therm. Eng. 29 (2–3) (2009) 224–233.
[12] M. Li, A.C.K. Lai, Heat-source solutions to heat conduction in anisotropic media with application to pile and borehole ground heat exchangers, Appl. Energy 96 (2012) 451–458.
[13] M. Li, A.C.K. Lai, Review of analytical models for heat transfer by vertical ground heat exchangers (GHEs): a perspective of time and space scales, Appl. Energy 151 (2015) 178–191.
[14] Y. Yang, M. Li, Short-time performance of composite-medium line-source model for predicting responses of ground heat exchangers with single U-shaped tube, Int. J. Therm. Sci. 82 (2014) 130–137 https://doi.org/10.1016/j.ijthermalsci.2014.04.002.
[15] J. Blackwell, A transient-flow method for determination of thermal constants of insulating materials in bulk part I—theory, J. Appl. Phys. 25 (2) (1954) 137–144.
[16] W.F. Waite, L.Y. Gilbert, W.J. Winters, D.H. Mason, Estimating thermal diffusivity

and specific heat from needle probe thermal conductivity data, Rev. Sci. Instrum. 77 (4) (2006) 044904.
[17] L. Lamarche, B. Beauchamp, New solutions for the short-time analysis of geothermal vertical boreholes, Int. J. Heat Mass Transf. 50 (7–8) (2007) 1408–1419.
[18] P. Metz, A simple computer program to model three-dimensional underground heat flow with realistic boundary conditions, J. Sol. Energy Eng. 105 (1) (1983) 42–49.
[19] Y. Gu, D.L. O'Neal, An analytical solution to transient heat conduction in a composite region with a cylindrical heat source, J. Sol. Energy Eng. 117 (3) (1995) 242–248.
[20] G. Bandyopadhyay, W. Gosnold, M. Mann, Analytical and semi-analytical solutions for short-time transient response of ground heat exchangers, Energy Build. 40 (10) (2008) 1816–1824.
[21] M.D. Mikhailov, M.N. Özişik, N.L. Vulchanov, Diffusion in composite layers with automatic solution of the eigenvalue problem, Int. J. Heat Mass Transf. 26 (8) (1983) 1131–1141.
[22] A. Haji-Sheikh, J.V. Beck, Temperature solution in multi-dimensional multi-layer bodies, Int. J. Heat Mass Transf. 45 (9) (2002) 1865–1877.
[23] D. Maillet, Thermal Quadrupoles: Solving the Heat Equation through Integral Transforms, John Wiley & Sons Inc, 2000.
[24] Technical information - polytetrafluoroethylene polytetrafluoroethylene PTFE, (2019) http://www.goodfellow.com/catalogue/GFCat2H.php?ewd_token=QyTGBL1K7e14OPElT7SvAejfQ1bDty&n=krjr2hZewT9mQyqnNN1FVhT4nNzToZ&ewd_urlNo=GFCat2L3&Head=FP30 , Accessed date: 23 January 2019.
[25] J. Blumm, A. Lindemann, M. Meyer, C. Strasser, Characterization of PTFE using advanced thermal analysis techniques, Int. J. Thermophys. 31 (10) (2010) 1919–1927.
[26] B.F. Blackwell, W. Gill, K. Dowding, T.E. Voth, Determination of thermal conductivity of 304 stainless steel using parameter estimation techniques, Sandia National Labs, Sandia National Labs, Albuquerque, NM (US), 2000.
[27] R.S. Graves, T.G. Kollie, D.L. McElroy, K.E. Gilchrist, The thermal conductivity of AISI 304L stainless steel, Int. J. Thermophys. 12 (2) (1991) 409–415.
[28] F. Reisdorffer, B. Garnier, N. Horny, C. Renaud, M. Chirtoc, T.-P. Nguyen, Thermal conductivity of organic semi-conducting materials using 3 omega and photothermal radiometry techniques, EPJ Web Conf. 79 (2014).
[29] R. Celorrio, A. Mendioroz, E. Apiñaniz, A. Salazar, C. Wang, A. Mandelis, Reconstruction of radial thermal conductivity depth profile in case hardened steel rods, J. Appl. Phys. 105 (8) (2009) 083517.